

A New Approach To Estimate The Collision Probability

Richard Altendorfer and Christoph Wilkmann

Abstract—We revisit the computation of probability of collision in the context of automotive collision avoidance (the estimation of a potential collision is also referred to as conflict detection in other contexts). After reviewing existing approaches to the definition and computation of a collision probability we argue that the question "What is the probability of collision within the next three seconds?" can be answered on the basis of a collision probability rate. Using results on level crossings for vector stochastic processes we derive a general expression for the upper bound of the distribution of the collision probability rate. This expression is valid for arbitrary prediction models including process noise. We demonstrate in several examples that distributions obtained by large-scale Monte-Carlo simulations obey this bound and in many cases approximately saturate the bound.

We derive an approximation for the distribution of the collision probability rate that can be computed on an embedded platform. In order to efficiently sample this probability rate distribution for determination of its characteristic shape an adaptive method to obtain the sampling points is proposed. An upper bound of the probability of collision is then obtained by one-dimensional numerical integration over the time period of interest. We also argue that temporal collision measures such as time-to-collision should not be calculated as separate or even prerequisite quantities but that they are properties of the distribution of the collision probability rate.

I. INTRODUCTION

The implementation of a collision mitigation or collision avoidance system requires in general the computation of a measure of criticality in order to assess the current traffic situation as well as its evolution in the short-term future. There are many criticality measures available, for example time-to-go (TTG) or time-to-collision (TTC), see e. g. [1],[2], or the brake threat number see e. g. [3]. All those measures are based on models of varying degrees of complexity of touching or penetrating the boundary of the potential colliding object, e. g. both the $TTC = -\frac{x(0)}{\dot{x}(0)}$ (for a constant velocity model) and the brake threat number $a_{req} = -\frac{\dot{x}^2(0)}{2\dot{x}(0)}$ are based on the one-dimensional collision event $x(t) = 0$.

Here we focus on this underlying collision event – the boundary penetration – in a fully probabilistic manner, i. e. we propose a new approach to compute the collision probability. The use of this collision probability for decision making in collision mitigation or avoidance systems is not subject of this investigation.

There are two fundamentally different approaches to computing a collision probability that are known to the authors:

- 1) probability of the spatial overlap of the host vehicle with the colliding vehicle's probability distribution, see e. g. [4], [5], and
- 2) probability of penetrating a boundary around the host vehicle, see e. g. [6],[7].

There is currently no satisfying way to compute the collision probability over a time period: there is a heuristic proposal to pick the maximal collision probability over that period as the collision probability for that time period [6],[1], and there are calculations relying on strong assumptions (e. g. constant velocity models) that directly compute the collision probability over a time period [6],[7].

In the following we will derive an expression for the upper bound of the probability of penetrating a boundary around the host vehicle in a time period $\Delta T = [t_1, t_2]$. This will be the result of the temporal integration of an upper bound of the probability *rate* for which we derive a general expression valid for arbitrary prediction models including process noise. Inclusion of process noise is crucial for collision avoidance systems since it allows to encode the uncertainty in the relative motion of the host and the colliding vehicle. This uncertainty is particularly relevant for predictions over several seconds where it is unknown whether the colliding vehicle keeps its motion, accelerates or slows down, or whether the host vehicle driver perceives the risk and slows down, for example.

The basis of our derivations are the time-dependent distributions $p_t(x, y, \dot{x}, \dot{y}, \dots)$, $t \in \Delta T$. Those distributions characterize a non-stationary vector stochastic process that represents the predicted relative state $\xi^-(t)$ of the colliding vehicle. The stochastic process can be the result of a dynamical system whose flow f can depend upon the state ξ , a time-dependent control input $u(t)$, process noise $\nu(t)$, and time t :

$$f(\xi, u(t), \nu(t), t) \quad (1)$$

In the remainder of this paper the time dependence of $\xi^-(t)$ and its elements will be suppressed, however the temporal dependence of probability distributions will be indicated by $p \rightarrow p_t$ where appropriate.

In the next section Monte-Carlo simulations of two collision scenarios are performed and it is shown that the result is naturally represented by a collision probability rate.

II. THE COLLISION PROBABILITY GROUND TRUTH: LARGE-SCALE MONTE-CARLO SIMULATIONS

Here, we want to investigate two examples of possible collision scenarios, one where the target vehicle is currently in front of the host vehicle and one where it is on the front right side. In order to obtain ground truth data for the future collision probability Monte-Carlo simulations are performed. The target vehicle on a possibly colliding path with the host

R. Altendorfer is with Advanced Driver Assistance Systems, ZF, Germany
richard.altendorfer@zf.com
C. Wilkmann is with RWTH Aachen, Germany
Christoph.Wilkmann@rwth-aachen.de

vehicle is modeled by the state vector $\xi = (x \ y \ \dot{x} \ \dot{y} \ \ddot{x} \ \ddot{y})^\top$ and the dynamical system as specified in appendix B. The target vehicle is chosen to be detected by a radar sensor mounted at the middle of the front bumper of the host vehicle with standard radar measurements also specified in app. B. Note however that this state vector as well as the dynamical system specified in appendix B constitute just an example – the central results in section V-A hold for general non-stationary as well as non-Gaussian stochastic processes. In particular, the absence of assumptions on the stationarity of the stochastic process means that processes derived from more general dynamical system – including systems with explicit time dependence or time-dependent control inputs $u(t)$ – are covered.

The starting point for an individual simulation is a sample point in state space ξ_i^- where the target vehicle is some distance away from the host vehicle - either directly in front or coming from the right side, see fig. 1. This sample point is drawn from a multivariate distribution characterized by its mean vector and covariance matrix which is usually the output of a probabilistic filter that takes into account the history of all previous sensor measurements that have been associated with this object. Instead of arbitrarily picking specific values for this *initial* covariance matrix we take its values from steady state¹ at this mean vector using the discrete algebraic Riccati equation. An instance ξ_i^- of an initial state of the target vehicle is drawn as a sample of $\mathcal{N}(\xi^-; \mu_\xi^-, P_\infty^-)$. This state is predicted using the stochastic differential equation (30) until it crosses the host vehicle boundary or a certain time limit is exceeded. Hence: collision event = crossing of the target vehicle path with the host vehicle boundary. The time until the crossing is recorded and a new simulation with a new sample of initial conditions is started. Examples of colliding trajectories starting from an initial position in front of the host vehicle are depicted in fig. 1.

We have performed simulations of $N_{traj} = 3 \cdot 10^6$ trajectories for the two starting points. The result is represented by a histogram of the number of collisions that occur within a histogram bin, i. e. time interval, with respect to time.

Hence simulating colliding trajectories naturally leads to a collision probability *rate*.

An example is given in fig. 2 where the bins are normalized by the total number of trajectories N_{traj} and the chosen bin width of $dt = 0.05s$ to obtain a collision probability rate. In addition, the collision probability rate integrated by simple midpoint quadrature from 0 to time t is shown. In this example the probability of collision with the target vehicle exceeds 60% within the first 6s. The asymptotic value of the collision probability as $t \rightarrow \infty$ indicates the overall probability of collision over all times.

The main contribution of this paper will be to derive formulae to obtain bounds of the collision probability and collision probability rate for a general dynamical system. We will also show that these formulae in many cases not only

provide bounds but accurate approximations by comparing the applied formulae with Monte-Carlo simulations using the specific scenarios described in this section.

In the following two sections we will review existing approaches to computing a collision probability.

III. COLLISION PROBABILITY FROM 2D SPATIAL OVERLAP

This is the probability of the spatial overlap between the host vehicle and the colliding vehicle as proposed in [4], [5]. In [4] the variables of the relevant probability distribution are either defined by the relative two-dimensional position and relative orientation (x, y, ψ) , or by the distribution of the difference of independent probability distributions of global two-dimensional position and orientation as in [5]. It is not explained how higher order derivatives necessary for prediction such as \dot{x}, \dot{y}, \dots have been dealt with (e. g. by marginalization).

Then in [4] the collision probability is obtained as the integral over the pdf of relative position and orientation over a collision volume D

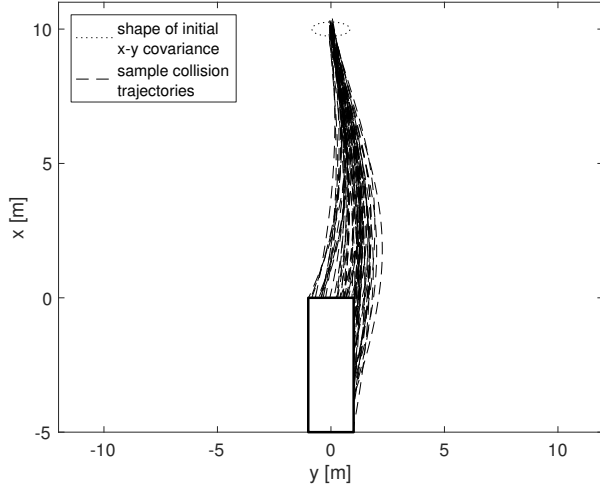
$$P_C(t) = \iiint_{x,y,\psi \in D} p(x, y, \psi) dx dy d\psi \quad (2)$$

which in turn is approximated as the convolution of independent probability distributions of global two-dimensional position of both host and colliding vehicle - orientation is ignored. Note that even this two-dimensional integral, i. e. the cumulative distribution function of a bivariate Gaussian, cannot be solved in closed form; however, numerical approximation schemes exist [8]. By further ignoring the $x-y$ -covariance the multivariate Gaussian decouples so that integration can be factored into one-dimensional Gaussian distributions [4]. In [5], the collision probability is computed as the integral of the product of the two global distributions.

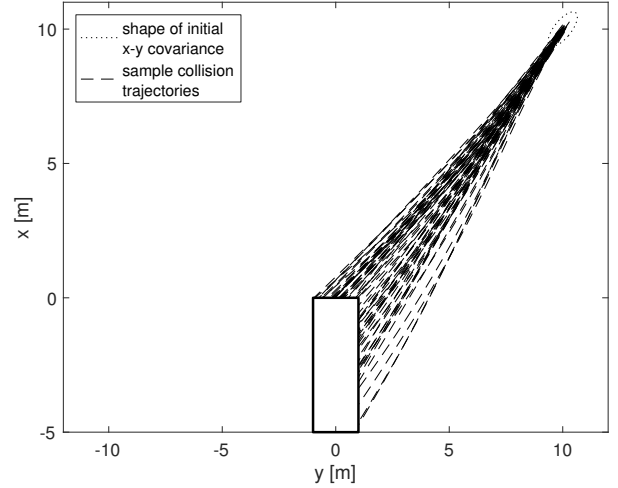
A problem of deriving a collision probability from 2D spatial overlap is that this approach directly yields a collision probability for a specific time, see fig. 3. Hence it does not allow to answer the question "What is the probability of collision within the next three seconds?" because integration of the collision probability over time does not yield a collision probability over a certain time period as already pointed out in [7]. In particular, time is not a random variable that can be marginalized over and an integral over a time interval ΔT : $\int_{\Delta T} P_C(t) dt$ has dimension of time and does not constitute a probability. A heuristic proposal to solve this problem has been to pick the maximal collision probability over a time period as the collision probability for that period [6],[1].

Another issue is that the collision probability is determined by the presence of the colliding object anywhere inside the entire area of the host vehicle. It could, for example be in the center of the host vehicle, which would be a catastrophic event and too late for collision avoidance, see fig. 3 for an example where the maximum of the instantaneous collision probability from spatial overlap occurs after the TTC in x-direction. What we are actually interested in is the probability of the colliding object touching and/or penetrating the boundary of the host vehicle. This requires a different approach than integration over state space as in eq. (2) since the integral over a lower-dimensional subspace would always be zero. Some existing

¹Strictly speaking there is no steady state at those points since the system is non-linear and the relative speed is not zero. Nevertheless the solution of the Riccati equation is still representative if the filter settles within a smaller time period than the time period in which the state changes significantly.



(a) The target is coming from the front $(\mu_x, \mu_y) = (10, 0) m$. The parameters for the time-dependent input as specified in app. B are $b_1 = -0.2ms^{-3}$, $b_2 = -0.3ms^{-3}$, $\omega = 0.5s^{-1}$.



(b) The target is coming from the front right $(\mu_x, \mu_y) = (10, 10) m$. The parameters for the time-dependent input as specified in app. B are $b_1 = -0.4ms^{-3}$, $b_2 = -0.5ms^{-3}$, $\omega = 0.5s^{-1}$.

Fig. 1. Samples of simulated colliding trajectories for vehicles initially coming from the front (a) and from the front right (b) side.

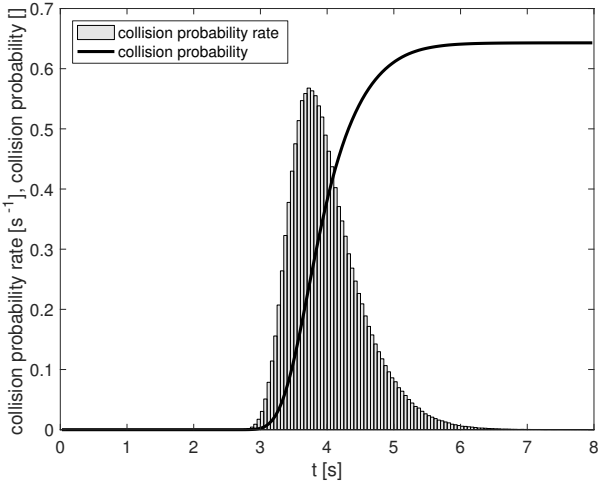


Fig. 2. Collision probability rate as a function of time for $(\mu_x, \mu_y) = (10, 0) m$ based upon $N_{traj} = 3 \cdot 10^6$ trajectories. Also shown is the collision probability obtained by integrating over time.

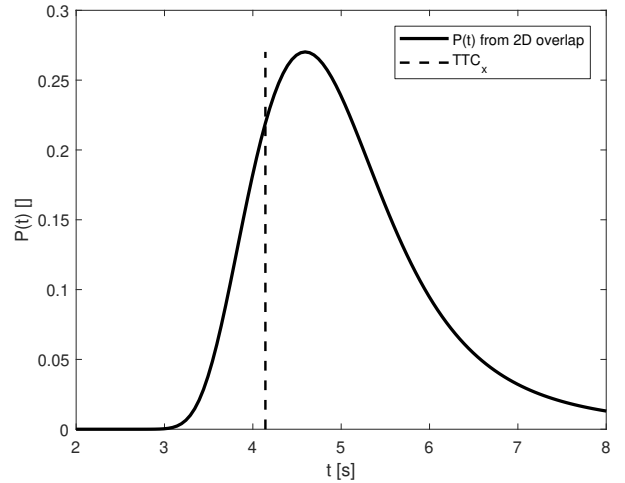


Fig. 3. Example of an instantaneous collision probability over time derived from a collision defined by spatial overlap as described in section III. This is based on the first scenario described in sec. II with initial condition in front of the host vehicle.

approaches that consider a boundary instead of a state space volume for the computation of a collision probability are reviewed in the next section.

IV. COLLISION PROBABILITY AT BOUNDARY

A probabilistic approach to computing the probability of penetrating a boundary - instead of the probability of a spatial overlap - has been proposed in [7]. Their method is based on the probability density of a so-called *time-to-go* which is the time to cross a straight, axis-aligned boundary assuming a constant velocity model. The derived collision probability refers to a time period and not just a time instant. It is only applicable to straight paths or combinations of piecewise straight paths and does not take into account more complex geometries such as a rectangle. It also relies on a separation of longitudinal and lateral motion. Another limitation is that

the stochastic nature of their conflict detection approach only comes from the distribution of the initial condition of their state $(x \ y \ \dot{x} \ \dot{y})^T$ - process noise is not considered. Although a central result on level crossings, albeit in one dimension, - namely Rice's formula, see e. g. [9] - is cited, it is not used in its original context to compute the intensity of crossings of a scalar variable but as a technical tool to derive the quotient distribution (for time-to-go) of two correlated random variables.

A somewhat complementary approach is taken in [6] for aircraft conflict detection in the sense that process noise is incorporated whereas the uncertainty of the initial condition is not. They propose two different algorithms, one for mid-range and one for short-range conflict detection. For mid-range conflict detection their measure of criticality is an instantaneous

probability of conflict and similar to the 2D spacial overlap discussed in the previous section. It is computed by a specific Monte-Carlo scheme.

On the other hand their short-range conflict detection is based on the penetration of a spherical boundary around the aircraft as criticality measure. The dynamics is a constant velocity model perturbed by Brownian motion. Their closed-form expression for a collision probability over a time period requires additional assumptions, the strongest of which are the assumed decoupling of the 2D motion into separate 1D motions in longitudinal and lateral directions and the formulation of the collision probability P_C over a time period $[0, t_f]$ as a factorization into a probability density $p_\tau(t)$ of the minimal time to cross a threshold along a one-dimensional, longitudinal direction² and the distribution of a one-dimensional Wiener process $p_{Lateral}(y, t)$ along the lateral direction:

$$P_C(0, t_f) \approx \int_0^{t_f} p_\tau(t) \int_{Lat. \text{ conflict width}} p_{Lateral}(y, t) dy dt \quad (3)$$

The many strong assumptions, in particular constant velocity motion, specific Brownian noise model, and decoupling into one-dimensional motions make this approach hard to generalize.

A different, semi-probabilistic approach is taken in [2] where the time-to-collision of a 2D constant velocity model with respect to the host vehicle's front boundary at $x = 0$ is computed. This TTC is then inserted into the prediction equation to arrive at

$$\begin{pmatrix} x + t\dot{x} \\ y + t\dot{y} \\ \dot{x} \\ \dot{y} \end{pmatrix} \rightarrow \begin{pmatrix} 0 \\ y - \frac{x}{\dot{x}}\dot{y} \\ \dot{x} \\ \dot{y} \end{pmatrix} \quad (4)$$

Then the second component of this vector is singled out and interpreted as a probabilistic expression. Its distribution as a function of the initial condition is determined by Monte-Carlo simulation and integrated over the host vehicle's front boundary to obtain a collision probability at the TTC. More complex geometries as well as process noise are not considered.

The approaches discussed above are limited to constant velocity models with assumptions on the coupling of longitudinal and lateral motion, they either incorporate specific process noise or no process noise at all or exclude the uncertainty of the initial condition. Additionally, they all rely on a time-to-go or TTC as a prerequisite quantity - either probabilistic or non-probabilistic. As we will show in the next section, such a temporal collision measure is not necessary for the computation of a collision probability. Instead, we show that a fundamental quantity to compute the collision probability for stochastic processes is the collision probability *rate*.

²Using a result on the temporal distribution of the crossing of a threshold for a one-dimensional constant velocity model perturbed by Brownian motion (sometimes referred to as Bachelier-Levy, see e. g. [10]).

V. COLLISION PROBABILITY RATE AT BOUNDARY

A. Derivation of an upper bound for the collision probability rate

We have seen that simulating colliding trajectories naturally gives us a probability rate and that a collision probability rate allows us to perform temporal integration to arrive at a collision probability for an extended period of time. An expression for the upper bound of the collision probability rate will be derived on the basis of a theorem on boundary crossings of stochastic vector processes. For sake of lucidity of arguments we restrict ourselves to one of the four straight boundaries of the host vehicle, see fig. 4; extension to the other boundaries is straightforward.

We start with the prediction of the pdf of a state vector that at least contains relative position and its derivative, i. e. $\xi = (x \ y \ \dot{x} \ \dot{y} \ \dots)^\top$ for a two-dimensional geometry, of a colliding object from an initial condition at $t = 0$ to a future time t where process noise $\nu(t)$ is explicitly incorporated:

$$\text{prediction : } p_0(x, y, \dot{x}, \dot{y}, \dots) \xrightarrow{t, \nu(t)} p_t(x, y, \dot{x}, \dot{y}, \dots) \quad (5)$$

Note that we do not make any assumptions on the used prediction model as well as noise model or explicit temporal dependencies, hence the stochastic dynamical system that gives rise the pdf could also explicitly depend upon time or a time-dependent control input $u(t)$. In order to cast the following expressions into a more readable format we define a probability distribution that only depends upon relative position and its derivative by marginalization (see app. A for marginalization of Gaussian densities, for example) of the predicted pdf over the other variables:³

$$p_t(x, y, \dot{x}, \dot{y}) := \int_{\text{other var.}} p_t(x, y, \dot{x}, \dot{y}, \text{other var.}) d(\text{other var.}) \quad (6)$$

Given the pdf $p_t(x, y, \dot{x}, \dot{y})$ what we are looking for is an expression for

$$\frac{dP_C^+}{dt}(\Gamma_{front}, t) \quad (7)$$

i. e. the collision probability rate $\frac{dP_C^+}{dt}$ with dimension $[s^{-1}]$ at time t for the front boundary Γ_{front} . The superscript + is used to denote that this probability rate is referring to boundary crossings from outside to inside.

1) *An Intuitive Motivation:* We start with the probability of the colliding object being inside an infinitesimally thin strip at the boundary Γ_{front} (see fig. 4)

$$dP_C^+(\Gamma_{front}, t) = \int_{y \in I_y} \int_{\dot{x} \leq 0} \int_{\dot{y} \in \mathbb{R}} p_t(x_0, y, \dot{x}, \dot{y}) dx dy d\dot{x} d\dot{y}$$

Here, since we are only interested in colliding trajectories, i. e. trajectories that cross the boundary from outside to inside,

³The state vector $\xi = (x \ y \ \dot{x} \ \dot{y} \ \ddot{x} \ \ddot{y})^\top$ specified in app. B is an obvious extension of the minimal state vector above with corresponding white noise jerk model described in eq. (30) and is used as an example to illustrate the computation of collision probability rate. It is however by no means specific to the results stated in this paper.

we do not fully marginalize over \dot{x} but restrict the x -velocity to negative values at the boundary.

A collision probability rate can now be obtained by dividing the unintegrated differential dx by dt ; in that way the “flow” of the target vehicle through the host vehicle boundary is described at x_0 with velocity $\dot{x} \leq 0$:

$$\frac{dP_C^+}{dt}(\Gamma_{front}, t) \simeq - \int_{y \in I_y} \int_{\dot{x} \leq 0} \int_{\dot{y} \in \mathbb{R}} p_t(x_0, y, \dot{x}, \dot{y}) \dot{x} dy d\dot{x} d\dot{y} \quad (8)$$

Here, since the velocity is restricted to negative values a minus sign is required to obtain a positive rate.

2) Derivation based upon the theory of level crossings:

This intuitive derivation can be amended as well as generalized in a mathematically rigorous way by invoking a result on crossings of a surface element by a stochastic vector process stated in [11]. First we need to set up the notations and definitions for entries and exits (level crossings) across the boundary of a region.

Let $\zeta(t)$ be a continuously differentiable n -dimensional vector stochastic process with values $\mathbf{x} \in \mathbb{R}^n$. The probability densities $p_t(\mathbf{x})$ and $p_t(\dot{\mathbf{x}}, \mathbf{x})$ exist where $\dot{\mathbf{x}} \in \mathbb{R}^n$ are the values of $\zeta(t)$. Let the region $S \in \mathbb{R}^n$ be bounded by the smooth surface ∂S defined by the smooth function g as $\partial S = \{\mathbf{x} : g(\mathbf{x}) = 0\}$ and let $\Gamma \subseteq \partial S$ be a subset of that surface. Let $\mathbf{n}_\Gamma(\mathbf{x})$ be the surface normal at \mathbf{x} directed towards the interior of the region.

A sample function $\mathbf{x}(t)$ of $\zeta(t)$ has an entry (exit) across the boundary Γ at t_0 if $g(\mathbf{x}) > 0$ ($g(\mathbf{x}) < 0$) $\forall t \in (t_0 - \epsilon, t_0)$ and $g(\mathbf{x}) < 0$ ($g(\mathbf{x}) > 0$) $\forall t \in (t_0, t_0 + \epsilon)$ for some $\epsilon > 0$. For a temporal interval $\Delta T = [t_1, t_2]$ the number of entries/exits across Γ in this interval is denoted by $N^\pm(\Gamma, t_1, t_2)$.

The importance of this mathematical setup is that using the number of entries a collision probability over ΔT can be defined as

$$P_C^+(\Gamma, t_1, t_2) := P(g(x(t_1)) \geq 0, N^+(\Gamma, t_1, t_2) \geq 1) \leq P(N^+(\Gamma, t_1, t_2) \geq 1) \quad (9)$$

i. e. the probability that the stochastic process enters the boundary in ΔT at least once with initial value outside the boundary. The probability that the process is outside the boundary at initial time t_1 should be almost one: $P(g(x(t_1)) \geq 0) \approx 1$ in automotive applications where a collision probability is to be computed for a time interval that begins at a time when the collision has not happened yet.

The first moment of $N^+(\Gamma, t_1, t_2)$ can be used to obtain an upper bound for $P(N^+(\Gamma, t_1, t_2) \geq 1)$:

$$P(N^+(\Gamma, t_1, t_2) \geq 1) \leq E\{N^+(\Gamma, t_1, t_2)\} \quad (10)$$

This becomes obvious by writing out the expressions above:

$$P(N^+ \geq 1) = \sum_{k=1}^{\infty} P(N^+ = k) \leq \sum_{k=0}^{\infty} k P(N^+ = k) = E\{N^+\} \quad (11)$$

It also shows that if the probabilities for two or more entries are much smaller than for one entry then $E\{N^+(\Gamma, t_1, t_2)\}$ is not just an upper bound but a good approximation to $P(N^+(\Gamma, t_1, t_2) \geq 1)$.

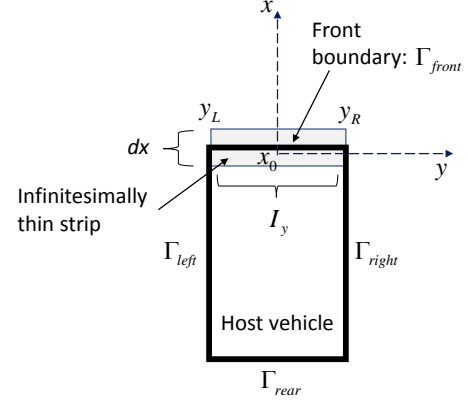


Fig. 4. Horizontal view of the host vehicle rectangle with local Cartesian coordinate system and coordinate origin at the middle of the front boundary characterized by $x = 0$ and $y \in [y_L, y_R] = I_y$.

It remains to compute the first moments for entry and exit which can be obtained via temporal integration of the entry/exit intensities μ^\pm as defined below:

$$\int_{t_1}^{t_2} \mu^\pm(\Gamma, t) dt := E\{N^\pm(\Gamma, t_1, t_2)\} \quad (12)$$

By combining eqs. (9) and (10) and evaluating the temporal derivative with respect to t_2 at t_1 we obtain

$$\frac{dP_C^+}{dt}(\Gamma, t_1) \leq \mu^+(\Gamma, t_1) \quad (13)$$

i. e. we have derived an upper bound for the collision probability rate.

This upper bound can be further evaluated using the explicit expression for the entry/exit intensities μ^\pm from [11]:

$$\mu^\pm(\Gamma, t) = \int_{\mathbf{x} \in \Gamma} E\left\{\langle \mathbf{n}_\Gamma(\mathbf{x}), \dot{\zeta}(t) \rangle^\pm \mid \zeta(t) = \mathbf{x}\right\} p_t(\mathbf{x}) ds(\mathbf{x}) \quad (14)$$

where $\langle \cdot, \cdot \rangle$ is the scalar product, $ds(\mathbf{x})$ is an infinitesimal surface element of Γ at \mathbf{x} and $(\cdot)^+ := \max(\cdot, 0)$ and $(\cdot)^- := -\min(\cdot, 0)$. Equation (14) holds for general non-Gaussian as well as non-stationary stochastic processes.

In order to apply eq. (14) to the front boundary Γ_{front} as in fig. 4 we need to perform the following identifications:⁴

$$\begin{aligned} \zeta(t) &= (x, y)^\top \\ \Gamma_{front} &= \{(x, y) : x - x_0 = 0 \wedge y \in I_y\} \\ g_{\Gamma_{front}}(\mathbf{x}) &= x - x_0 \\ \mathbf{n}_{\Gamma_{front}}(\mathbf{x}) &= (-1, 0)^\top \\ ds_{\Gamma_{front}}(\mathbf{x}) &= dy \end{aligned} \quad (15)$$

Hence we obtain for the intermediate expectation operator

$$E\left\{\langle \mathbf{n}_{\Gamma_{front}}(\mathbf{x}), \dot{\zeta}(t) \rangle^+ \mid \zeta(t) = \mathbf{x}\right\} = - \int_{\dot{x} \leq 0} \int_{\dot{y} \in \mathbb{R}} \dot{x} p_t(\dot{x}, \dot{y} | x, y) d\dot{x} d\dot{y} \quad (16)$$

⁴From now on we do not distinguish anymore between a stochastic process and its sample values.

and the entry intensity becomes⁵

$$\begin{aligned} \mu^+(\Gamma_{front}, t) &= -\int \left(\int_{y \in I_y} \int_{\dot{x} \leq 0} \int_{\dot{y} \in \mathbb{R}} \dot{x} p_t(\dot{x}, \dot{y} | x_0, y) d\dot{x} d\dot{y} \right) p_t(x_0, y) dy \\ &= -\int_{y \in I_y} \int_{\dot{x} \leq 0} \int_{\dot{y} \in \mathbb{R}} \dot{x} p_t(x_0, y, \dot{x}, \dot{y}) dy d\dot{x} d\dot{y} \quad (17) \end{aligned}$$

This shows that the intuitive derivation of the collision probability rate (eq. (8)) results in the correct expression for the upper bound. It should be noted, however, that the application of the formalism above to a rectangular boundary of the host vehicle is just an example. By the theorem stated above the formula can be applied to any subsets of smooth surfaces, including higher dimensional ones for three-dimensional objects, for example. In app. D the formula for the entry intensity has been derived for a circular boundary.

The computation above applies to the front boundary of the host vehicle. In order to cover all four boundaries of the host vehicle the entry intensities of the four boundaries can be added since the crossing events through the different boundaries are mutually exclusive. Hence the total entry intensity is given by

$$\begin{aligned} \mu^+(\Gamma_{host\ vehicle}, t) &= \mu^+(\Gamma_{front}, t) + \mu^+(\Gamma_{right}, t) \\ &\quad + \mu^+(\Gamma_{left}, t) + \mu^+(\Gamma_{rear}, t) \quad (18) \end{aligned}$$

With these expressions the collision probability rate and collision probability for the surface subset Γ within a time interval $\Delta T = [t_1, t_2]$ are bounded by

$$\frac{dP_C^+}{dt}(\Gamma_{host\ vehicle}, t_1) \leq \mu^+(\Gamma_{host\ vehicle}, t_1) \quad (19)$$

$$P_C^+(\Gamma_{host\ vehicle}, t_1, t_2) \leq \int_{t_1}^{t_2} \mu^+(\Gamma_{host\ vehicle}, t) dt \quad (20)$$

Note that the stochastic process ξ representing the state of the colliding object needs to contain 2D relative position $(x\ y)^\top$ and 2D relative velocity $(\dot{x}\ \dot{y})^\top$. In many ADAS applications the target vehicle dynamics is modeled directly in relative coordinates. For state vectors that do not contain the 2D relative velocity but other quantities such as the velocity over ground (see e. g. [12]), a probabilistic transformation to relative velocities must be performed first. Indeed, modeling the host and target vehicle's motion over ground individually, e. g. by the well-known differential equation for the CTRA model, and then deriving a differential equation for an appropriately defined "relative" dynamics [12] leads to a more realistic motion description.

B. Implementation for Gaussian distributions

For further computations - especially in the Gaussian case - it will be convenient to marginalize over \dot{y} and rewrite eq.

⁵Because of the simple projection of the velocity onto the surface normal $(\mathbf{n}_{\Gamma_{front}}(\mathbf{x}), \zeta(t))^+ = -\dot{x}$ for the front boundary this expression could be further simplified by marginalization over \dot{y} .

(17) in terms of a conditional probability:

$$\mu^+(\Gamma_{front}, t) = -p_t(x_0) \int_{\dot{x} \leq 0} \int_{y \in I_y} \dot{x} p_t(\dot{x}, y | x_0) d\dot{x} dy \quad (21)$$

For general distribution functions the integral in eq. (21) cannot be computed in closed form and numerical integration methods must be used. Even in the bivariate Gaussian case there is no explicit solution known to the authors. However, by a Taylor-expansion with respect to the off-diagonal element of the inverse covariance matrix of $p(y, \dot{x} | x_0)$ as detailed in app. C, the integral can be factorized into one-dimensional Gaussians and solved in terms of the standard normal one-dimensional cumulative distribution function Φ . To zeroth order the integration yields:

$$\begin{aligned} \mu^+(\Gamma_{front}, t) &= -\mathcal{N}(x_0; \mu_x, \sigma_x) \\ &\quad \cdot \left(\left(\mu_{\dot{x}|x_0} \Phi \left(\frac{-\mu_{\dot{x}|x_0}}{\tilde{\sigma}_{\dot{x}|x_0}} \right) \right. \right. \\ &\quad \left. \left. - \tilde{\sigma}_{\dot{x}|x_0}^2 \mathcal{N}(0; \mu_{\dot{x}|x_0}, \tilde{\sigma}_{\dot{x}|x_0}) \right) \right. \\ &\quad \cdot \left(\Phi \left(\frac{y_R - \mu_{y|x_0}}{\tilde{\sigma}_{y|x_0}} \right) - \Phi \left(\frac{y_L - \mu_{y|x_0}}{\tilde{\sigma}_{y|x_0}} \right) \right) \\ &\quad \left. + \mathcal{O}(\Sigma_{12}^{-1}) \right) \quad (22) \end{aligned}$$

Here, if $\Sigma \in \mathbb{R}^{2 \times 2}$ is the covariance matrix of $p(\dot{x}, y | x_0)$, then $\tilde{\sigma}_{\dot{x}|x_0} = \sqrt{\frac{|\Sigma|}{\Sigma_{yy}}}$ and $\tilde{\sigma}_{y|x_0} = \sqrt{\frac{|\Sigma|}{\Sigma_{\dot{x}\dot{x}}}}$, see app. C where the integration has also been carried out to first order in Σ_{12}^{-1} . Expression (22) can be computed on an embedded platform using the complementary error function available in the C math library.⁶

In the next section an extensive numerical study using the above formulae and Monte-Carlo simulations is presented.

VI. NUMERICAL STUDY

A numerical study has been carried out to address the following questions:

- Is the expression for calculating the entry intensity from eq. (14) consistent with the results from large scale Monte-Carlo simulations?
- How does the approximation (22) perform in comparison with the numerical integration of the derived expression (21) for the entry intensity?
- Can the computational effort be reduced by increasing Δt and still accurately calculating the entry intensity?

A. *Is the upper bound of the collision probability rate corroborated by Monte-Carlo simulation?*

In order to address the first question, large scale Monte-Carlo simulations as described in sec. II have been performed. Entry intensities were calculated based on $3 \cdot 10^6$ sample trajectories for each of the two initial conditions $\mathcal{N}_i(\xi^-; \mu_{\xi^-}, P_{\infty}^-)$,

⁶ Φ is related to the error function erf and complementary error function erfc by $\Phi(x) = \frac{1}{2} \text{erfc} \left(\frac{-x}{\sqrt{2}} \right) = \frac{1}{2} - \frac{1}{2} \text{erf} \left(\frac{-x}{\sqrt{2}} \right)$.

where $\mu_{\xi_i}^-$ is shown in table I, and P_{∞}^- is calculated using the discrete Riccati equation with the matrices defined in appendix B. The two initial conditions ($i \in \{f, fr\}$) describe a starting point directly in front of the host vehicle, and in front to the right at an angle of 45 degrees with respect to the host vehicle.

TABLE I
MEAN OF INITIAL CONDITIONS FOR MONTE-CARLO SIMULATIONS

$\mu_{\xi_i}^-$	i	f	fr
$\mu_{\bar{x}}^- [m]$		10	10
$\mu_{\bar{y}}^- [m]$		0	10
$\mu_{\bar{\dot{x}}}^- [\frac{m}{s}]$		-2	-2
$\mu_{\bar{\dot{y}}}^- [\frac{m}{s}]$		0.4	-1.6
$\mu_{\bar{\ddot{x}}}^- [\frac{m}{s^2}]$		-0.2	-0.001
$\mu_{\bar{\ddot{y}}}^- [\frac{m}{s^2}]$		0.0	-0.01

Table II shows the number of collisions divided into the respective boundaries of the host vehicle where the impact or boundary crossing occurred for the two different simulations.

TABLE II
NUMBER OF COLLISIONS AT HOST VEHICLE BOUNDARIES FOR $3 \cdot 10^6$ SIMULATED TRAJECTORIES WITH DIFFERENT INITIAL CONDITIONS.

Γ_j	i	f	fr
$front$		$1.50 \cdot 10^6$	$8.31 \cdot 10^5$
$right$		$4.25 \cdot 10^5$	$1.39 \cdot 10^6$
$left$		0	0
$rear$		0	0
Σ		$1.93 \cdot 10^6$	$2.22 \cdot 10^6$

The resulting histograms of the collision probability rates are shown in fig. 5 together with the entry intensity obtained by numerical integration of the bivariate Gaussian in (21) as well as the difference between the simulation and the calculation. The difference is calculated by evaluating the entry intensity at the same time as the mid points of the histogram bins.

As can be seen in fig. 5, the entry intensity obtained by numerical integration of the exact expression (eq. (21)) accurately reproduces the collision probability rate from Monte-Carlo simulations. In order to illustrate the increase in accuracy as a function of the number of simulated trajectories, fig. 6 shows the differences between simulation and numerical integration with increasing amount of simulated trajectories for collisions at the right side of the host vehicle in the front scenario.

The reason why the entry intensity approximates the observed collision probability rates so well is the very low occurrence of higher order entries, i. e. entries where the trajectory enters the boundary more than once (see statistics of a Monte-Carlo simulation in table III). In the absence of higher order entries the expected number of entries becomes equal to the probability of entering the boundary at least once, see eq. (11). Since the corresponding time interval is arbitrary this equality propagates to an equality of the rates (compare to eq. (13)). In this context, we want to point out a subtlety concerning the number of entries regarding the

entire vehicle boundary $\Gamma_{host\ vehicle}$ versus entries through one of the boundary segments such as Γ_{right} . In Monte-Carlo simulations we have observed trajectories as shown in fig. 7 where the trajectory first enters the front boundary, exits the right boundary and then re-enters the right boundary again. With respect to the entire vehicle boundary $\Gamma_{host\ vehicle}$ this counts as a second entry – however with respect to the individual right boundary segment Γ_{right} this is a first entry. This is illustrated in fig. 8 where the entry intensity and Monte-Carlo histogram for Γ_{right} are plotted. Only by taking into account both the contributions from entries of trajectories that have never been inside $\Gamma_{host\ vehicle}$, i. e. first entries of $\Gamma_{host\ vehicle}$ and hence also first entries of Γ_{right} , as well as first (and possibly higher order) entries of Γ_{right} by trajectories from inside $\Gamma_{host\ vehicle}$ is the entry intensity properly approximated.

TABLE III
ABSOLUTE FREQUENCY H AND RELATIVE FREQUENCY P OF THE NUMBER OF ENTRIES N^+ OF COLLIDING TRAJECTORIES FOR $\Gamma_{host\ vehicle}$ BASED ON $1 \cdot 10^7$ SIMULATED TRAJECTORIES FOR $\Delta T = [0, 8s]$.

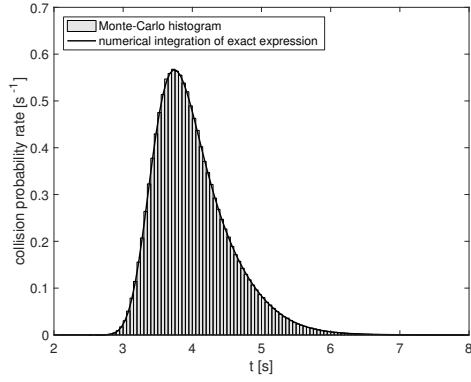
X	$\Gamma_{host\ vehicle}$	$H(X)$	$P(X)$	$\frac{P(X)}{P(N^+ \geq 1)}$
$N^+ = 1$		4, 493, 419	0.4493	0.9981
$N^+ = 2$		8, 772	0.0009	0.0019
$N^+ \geq 1$		4, 502, 191	0.4502	1

B. Does the approximation by Taylor-expansion accurately reproduce the exact result?

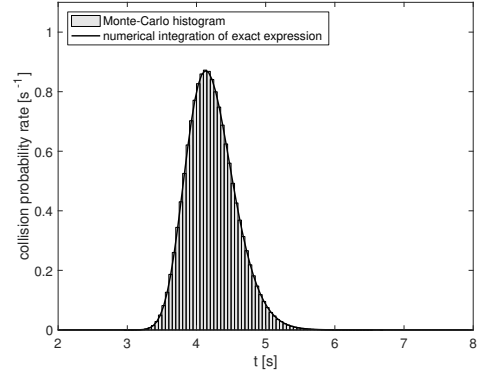
In order to be able to compute the entry intensity efficiently on an embedded platform, an approximation of the exact expression (eq. (17)) was derived in eq. (22). Fig. 9 shows the differences between this approximation as well as a higher-order approximation where the pdf is Taylor-expanded to linear order with respect to the off-diagonal element of the inverse covariance matrix around 0 (see app. C) and the numerical integration of (21). As can be seen, the higher-order approximation reduces the error to a large extent while it can be still calculated efficiently on an embedded platform using the complementary error function.

C. An adaptive method to sample the entry intensity over ΔT

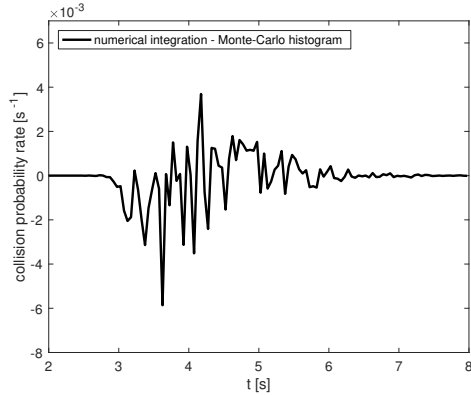
The approximations above of the exact expression of the entry intensity were evaluated at small time increments of $\Delta t = 0.05s$. Thus, the calculation over the entire time period of interest (e.g. $8s$ as used above) and for every relevant object could induce a substantial computational burden. In order to reduce this effort, we propose an adaptive method to sample the entry intensity function with variable – i. e. in general larger – time increments Δt over the time period of interest while still capturing the characteristics of this function, in particular its shape around the maximum. The sampling starting point is based upon the non-probabilistic TTCs for single, straight boundaries using a one-dimensional constant acceleration model. Those TTCs for penetrating the front, left, and right boundaries can then be used as initial condition



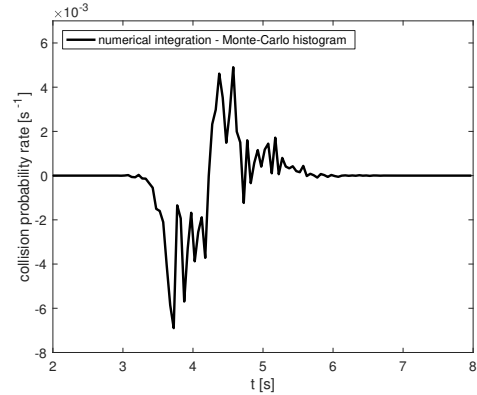
(a) Front scenario total collision probability rate and entry intensity



(b) Front-Right scenario total collision probability rate and entry intensity

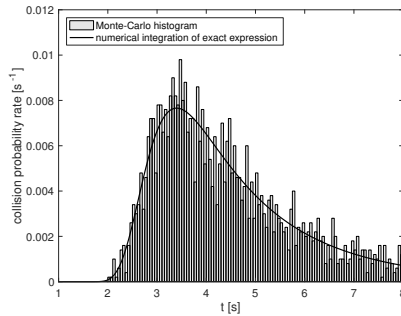


(c) Front scenario: difference between total collision probability rate and entry intensity

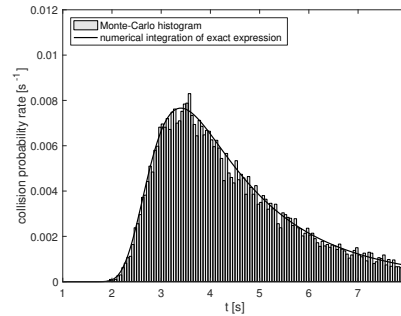


(d) Front-Right scenario: difference between total collision probability rate and entry intensity

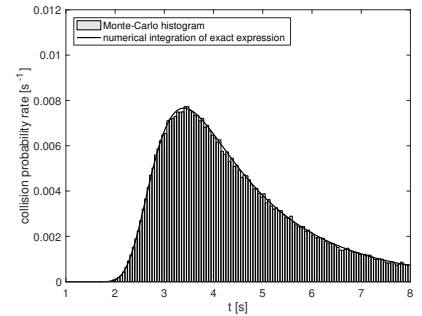
Fig. 5. The histogram resulting from Monte-Carlo simulation is shown together with the entry intensity obtained by numerical integration of the bivariate Gaussian for front (a) and front-right (b) scenario. The differences between simulation and numerical integration are calculated by evaluating the numerical integration at the same time as the mid points of the histogram bins and shown in (c) and (d).



(a) Simulation based on $1 \cdot 10^5$ trajectories.



(b) Simulation based on $1 \cdot 10^6$ trajectories.



(c) Simulation based on $1 \cdot 10^7$ trajectories.

Fig. 6. The collision probability rate for the right side of the host vehicle for the front scenario is shown comparing the results from Monte-Carlo simulation with increasing amount of simulated trajectories (a)-(c) with the entry intensity obtained by numerical integration of the bivariate Gaussian (eq. (21)). The process noise PSD for both coordinates is $\hat{q}_x = \hat{q}_y = 1.0125m^2s^{-5}$.

for the start of the sampling iteration of the entry intensity.⁷ To reproduce the entry intensity without substantial loss of information but with lower computational effort, the following algorithm is proposed:

- Calculate the times of penetrating the front, left and

⁷Due to the low probability of penetration the non-probabilistic TTC for the rear boundary is not considered for the determination of the sampling starting point.

right boundaries based upon the non-probabilistic TTCs described above.

- Calculate the entry intensity for each time. Pick the time with the maximum entry intensity as a starting point.
- Move left and right from this starting point with equally spaced $\Delta t_1 > \Delta t$ and calculate the entry intensity at these time points. Stop on each side if the entry intensity has reached a lower threshold of $\frac{dP_C^+}{dt} \text{ low}$.

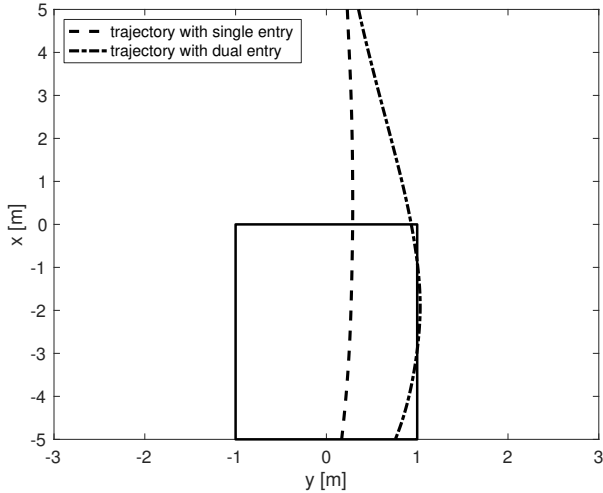


Fig. 7. Observed simulated trajectory entering the entire vehicle boundary $\Gamma_{host\ vehicle}$ once and trajectory entering twice.

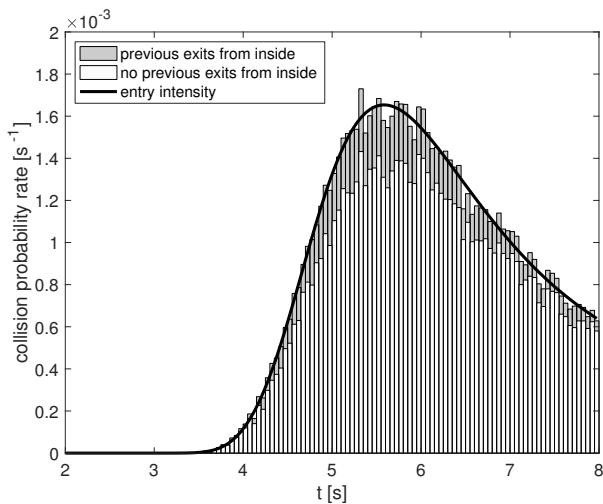


Fig. 8. The entry intensity of the right side Γ_{right} of the host vehicle for the front scenario is shown together with the Monte-Carlo histogram where entries by trajectories that have previously exited Γ_{right} from inside $\Gamma_{host\ vehicle}$ are marked in dark gray.

- While moving left and right, check if the slope of the entry intensity has changed its sign.
- On every slope sign change, calculate the entry intensity around this time interval with decreased $\Delta t_2 < \Delta t_1$.

Examples of this implementation can be found in fig. 10 for the front and front-right scenarios. It can be seen that the entry intensity as well as the entry intensity integrated over a certain time period can be determined with considerably fewer sampling points while still capturing the shape of the functions to be approximated.

VII. WHAT IS THE TTC?

There are various approaches to computing the TTC. In [2], the TTC is computed as the mean of the time distribution of reaching the x_0 boundary of the car as a function of the initial conditions assuming a constant speed model; process noise is not considered. This is also presented in [1]; in

addition the time distribution for reaching the x_0 boundary as a function of the initial conditions assuming a constant acceleration model is calculated by Monte-Carlo-simulation and its mean values depending upon the initial condition setup is given - again, process noise for this motion model is not considered. As a notable exception, in [3] the covariance of the distribution of TTC (or the related time-to-go in [7]) has been augmented by standard error propagation and judicious use of the implicit function theorem to include the effect of process noise. Nevertheless their TTC is still based on a reduction to a one-dimensional, longitudinal motion. As will be shown below these restricted temporal quantities do not fully capture the characteristics of horizontal plane collision scenarios.

In the following figures collision probability rates obtained by Monte-Carlo simulations as well as the entry intensities are plotted together with time-dependent jerk TTCs in x - and y -directions as the solution of the deterministic equations $x(t) = x_0$ and $y(t) = y_R$ based upon the time-dependent jerk input described in app. B.

These TTCs are also the mean values of distributions derived by promoting this deterministic expression (e. g. $TTC_x = -\frac{x(0)}{\ddot{x}(0)}$ for a simple linear velocity model) to a probability distribution due to the distribution of the initial condition and obtaining the mean by the usual first-order approximation of non-Gaussian densities.⁸

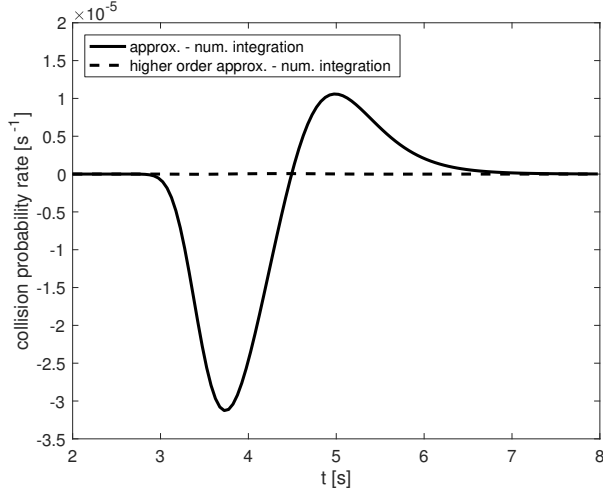
In fig. 11 the collision probability rate is plotted with the time-dependent jerk TTCs for the x - and y -directions for an initial position at the front, right side. Both TTCs in x - and y -direction are significantly different from the time of the maximum of the collision probability rate. Since the bulk of the colliding trajectories go through two sides - front and right (see also fig. 1b) - only a collision model that takes into account the full geometry of the host vehicle can yield accurate results.

In fig. 12 the collision probability rate is plotted together with the time-dependent jerk TTCs (i. e. their mean values) for the x -direction for an initial position that is straight in front of the vehicle hence almost all trajectories pass through the front boundary. Nevertheless the maximum of the probability rate bound occurs before the mean of the TTC. This difference increases as the process noise increases as can be seen in fig. 13. This is due to the fact that the time of the maximum is strongly influenced by the factor $p_t(x_0)$ in eq. (21); an increased level of process noise leads to a faster spreading of $p_t(x_0)$ and hence the maximum is reached earlier.

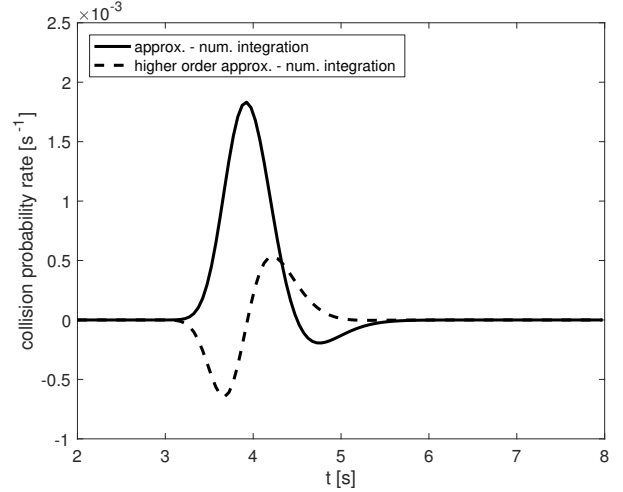
The above discussion shows that temporal collision characteristics are encoded by the distribution of the collision probability rate which incorporates the full geometry of the host vehicle as well as process noise during prediction.

A quantity called *TTC* could then be *defined* as one of the characteristic properties of this distribution such as the mode or the mean or the median, or as a property of the integrated collision probability rate, e. g. the time when the collision probability exceeds a certain threshold.

⁸Note that the augmented TTC-computation in [3] does not alter the mean but only the covariance.

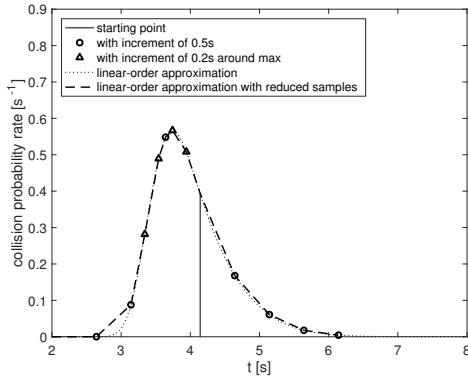


(a) Front scenario

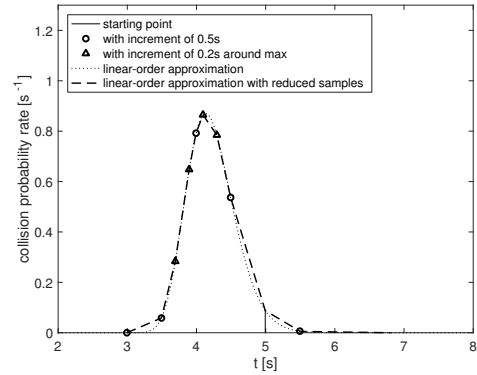


(b) Front-Right scenario

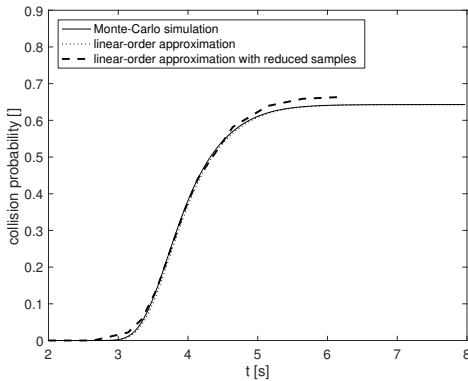
Fig. 9. Differences between numerical integration of the bivariate Gaussian in the expression of the entry intensity in eq. (21) and two approximations. The first approximation (solid line) ignores the non-diagonal entries of the covariance matrix while the second approximation (dashed line) Taylor-expands the pdf to linear order with respect to the off-diagonal elements of the inverse covariance matrix around 0.



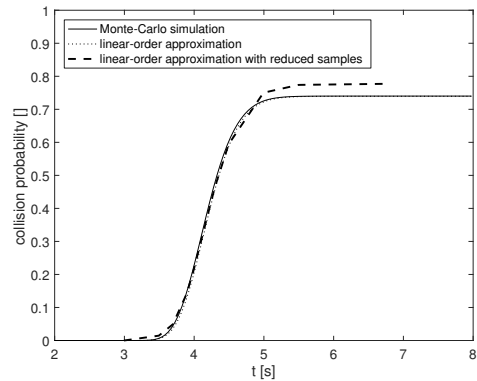
(a) Front scenario entry intensity



(b) Front-Right scenario entry intensity



(c) Front scenario integrated entry intensity



(d) Front-Right scenario integrated entry intensity

Fig. 10. Examples for reducing the number of calculations to determine the entry intensity and the integrated entry intensity. (a) and (c) show the results for the front scenario and (b) and (d) for the front-right scenario. The parameters in these examples are $\Delta t_1 = 0.5s$, $\Delta t_2 = 0.2s$ and $\frac{dP_C^+}{dt}|_{low} = 0.01$. In doing so the number of calculations for the entry intensity could be reduced from 120 (using a fixed sampling increment of $\Delta t = 0.05s$) to 13 for the front scenario and to 12 for the front-right scenario, respectively.

VIII. CONCLUSIONS

As detailed in our literature review a common approach to compute a collision probability is via temporal collision

measures such as time-to-collision or time-to-go. In this paper, however, we have pursued a different approach, namely the investigation of a collision probability rate without temporal

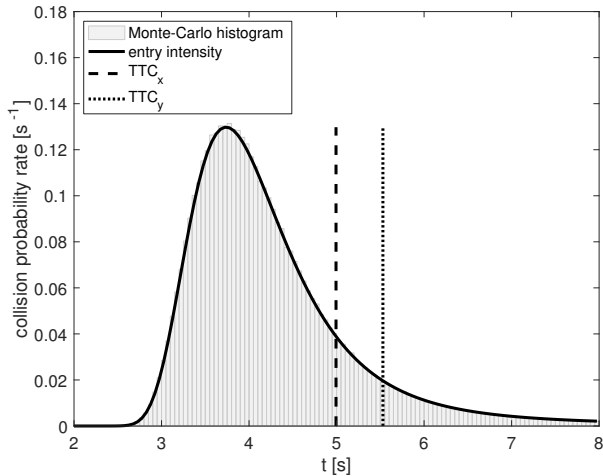


Fig. 11. Collision probability rate from Monte-Carlo simulation, entry intensity, and mean of time-dependent jerk TTC for an initial condition at the front, right side of the vehicle: $(x, y) = (10, 10)m$. The process noise PSD for both coordinates is $\tilde{q}_x = \tilde{q}_y = 0.4m^2s^{-5}$. The parameters for the time-dependent input as specified in app. B are $b_1 = -0.2ms^{-3}$, $b_2 = -0.1ms^{-3}$, $\omega = 0.5s^{-1}$.

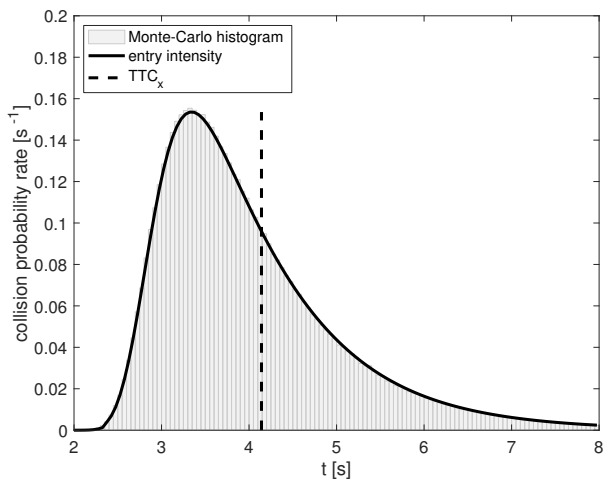


Fig. 12. Collision probability rate from Monte-Carlo simulation, entry intensity, and mean of time-dependent jerk TTC for an initial condition almost in front of the vehicle: $(x, y) = (10, 0)m$. The process noise PSD for both coordinates is $\tilde{q}_x = \tilde{q}_y = 0.0101m^2s^{-5}$. The parameters for the time-dependent input as specified in app. B are $b_1 = -0.2ms^{-3}$, $b_2 = -0.3ms^{-3}$, $\omega = 0.5s^{-1}$.

collision measures as an intermediate or prerequisite quantity. A collision probability rate then affords the provision of a collision probability over an extended period of time by temporal integration. An expression for an upper bound of the collision probability rate has been derived based on the theory of level crossings for vector stochastic processes. The condition under which the upper bound is saturated, i. e. is a good approximation of the collision probability rate has been discussed. While the expression was exemplified by an application of Gaussian distributions on a two-dimensional rectangular surface, the formalism holds for general non-stationary as well as non-Gaussian stochastic processes and can be applied to any subsets of multidimensional smooth surfaces. We have also shown that computations of TTCs using

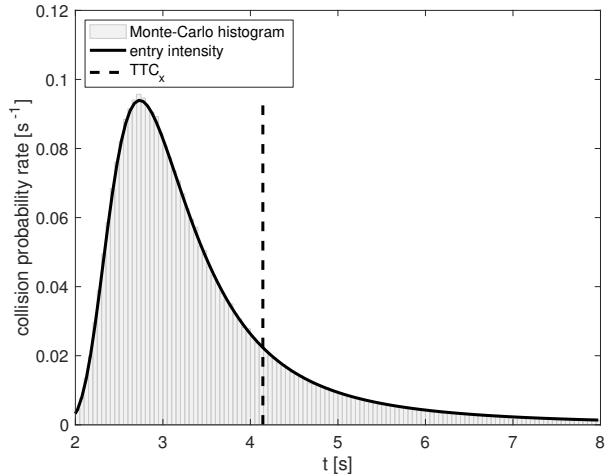


Fig. 13. Collision probability rate from Monte-Carlo simulation, entry intensity, and mean of time-dependent jerk TTC for an initial condition almost in front of the vehicle: $(x, y) = (10, 0)m$. The process noise PSD for both coordinates has been increased to $\tilde{q}_x = \tilde{q}_y = 1.0125m^2s^{-5}$. The parameters for the time-dependent input as specified in app. B are $b_1 = -0.2ms^{-3}$, $b_2 = -0.3ms^{-3}$, $\omega = 0.5s^{-1}$.

assumptions based on the shape of trajectories or the prediction dynamics (disregard of process noise), or on simple geometries such as a single line segment do not properly characterize the true collision probability rate distributions.

The ground truth collision probability rate distribution has been obtained by Monte-Carlo simulations and approximated by our derived bound for the collision probability rate. We have also implemented an approximation of the collision probability rate bound that can be computed in closed form on an embedded platform. This approximate formula provided bounds of the collision probability rate distributions that are almost indistinguishable from distributions obtained by numerical integration for the scenarios considered in this paper. In order to efficiently sample this probability rate distribution for determination of its characteristic shape we have worked out an adaptive method to obtain the sampling points.

IX. ACKNOWLEDGEMENTS

Helpful clarifications by Prof. Georg Lindgren are gratefully acknowledged.

APPENDIX

A. Partitioned Gaussian densities

In many calculations in stochastic estimation there is a need to marginalize over certain elements of a state vector or to obtain lower dimensional distributions by conditioning with respect to certain elements. For these calculations the original state vector ξ can be rearranged or partitioned such that x_r denotes the remaining state vector and x_m denotes the states to be marginalized over or which are used for conditioning.

$$\xi = \begin{pmatrix} x_r \\ x_m \end{pmatrix} \quad (23)$$

Hence the mean vector μ and covariance matrix Σ can be partitioned into

$$\mu = \begin{pmatrix} \mu_r \\ \mu_m \end{pmatrix}, \quad \Sigma = \begin{pmatrix} \Sigma_{rr} & \Sigma_{rm} \\ \Sigma_{rm}^\top & \Sigma_{mm} \end{pmatrix} \quad (24)$$

The following two well-known results on multivariate Gaussians are used in this paper:

a) *Marginalization*: The probability density of ξ marginalized with respect to x_m is

$$p(x_r) = \int_{x_m} p(\xi) dx_m = \mathcal{N}(x_r; \mu_r, \Sigma_{rr}) \quad (25)$$

b) *Conditioning*: The probability density of ξ conditioned on x_m is

$$\begin{aligned} p(\xi|x_m) &= p(x_r|x_m) \\ &= \mathcal{N}(x_r; \mu_{r|m}, \Sigma_{r|m}) \end{aligned} \quad (26)$$

with

$$\mu_{r|m} = \mu_r + \Sigma_{rm} \Sigma_{mm}^{-1} (x_m - \mu_m) \quad (27)$$

$$\Sigma_{r|m} = \Sigma_{rr} - \Sigma_{rm} \Sigma_{mm}^{-1} \Sigma_{rm}^\top \quad (28)$$

B. Dynamical system

The example vehicle kinematics is characterized by a six-dimensional state vector

$$\xi = (x \ y \ \dot{x} \ \dot{y} \ \ddot{x} \ \ddot{y})^\top \quad (29)$$

The continuous dynamics is given by a continuous white noise jerk model (see e. g. [13]) with additional time-dependent control input $u(t)$:

$$\dot{\xi} = F\xi + L\nu + Bu \quad (30)$$

where

$$F = \begin{pmatrix} 0 & 0 & 1 & 0 & 0 & 0 \\ 0 & 0 & 0 & 1 & 0 & 0 \\ 0 & 0 & 0 & 0 & 1 & 0 \\ 0 & 0 & 0 & 0 & 0 & 1 \\ 0 & 0 & 0 & 0 & 0 & 0 \\ 0 & 0 & 0 & 0 & 0 & 0 \end{pmatrix}$$

$$L = B = \begin{pmatrix} 0 & 0 \\ 0 & 0 \\ 0 & 0 \\ 0 & 0 \\ 1 & 0 \\ 0 & 1 \end{pmatrix}$$

and

$$u(t) = \begin{pmatrix} b_1 \sin(\omega t) \\ b_2 \sin(\omega t) \end{pmatrix}$$

Process noise ν is characterized by the jerk power spectral density (PSD) $\tilde{Q} = \text{diag}(\tilde{q}_x, \tilde{q}_y)$.

The discrete dynamics, i. e. the solution of this differential equation, can be obtained by standard linear system techniques. The covariance matrix of discrete-time equivalent process noise is given by (see e. g. [13])

$$Q(t_{k+1}, t_k) = \int_{t_k}^{t_{k+1}} \Phi(t_{k+1}, \tau) L \tilde{Q} L^\top \Phi^\top(t_{k+1}, \tau) d\tau \quad (31)$$

where Φ is the transition matrix of the homogeneous differential equation. The closed-form expression for this covariance matrix reads

$$Q(\Delta t_k) = \begin{pmatrix} \frac{\Delta t_k^5}{20} \tilde{q}_x & 0 & \frac{\Delta t_k^4}{8} \tilde{q}_x & 0 & \frac{\Delta t_k^3}{6} \tilde{q}_x & 0 \\ 0 & \frac{\Delta t_k^5}{20} \tilde{q}_y & 0 & \frac{\Delta t_k^4}{8} \tilde{q}_y & 0 & \frac{\Delta t_k^3}{6} \tilde{q}_y \\ \frac{\Delta t_k^4}{8} \tilde{q}_x & 0 & \frac{\Delta t_k^3}{3} \tilde{q}_x & 0 & \frac{\Delta t_k^2}{2} \tilde{q}_x & 0 \\ 0 & \frac{\Delta t_k^4}{8} \tilde{q}_y & 0 & \frac{\Delta t_k^3}{3} \tilde{q}_y & 0 & \frac{\Delta t_k^2}{2} \tilde{q}_y \\ \frac{\Delta t_k^3}{6} \tilde{q}_x & 0 & \frac{\Delta t_k^2}{2} \tilde{q}_x & 0 & \Delta t_k \tilde{q}_x & 0 \\ 0 & \frac{\Delta t_k^3}{6} \tilde{q}_y & 0 & \frac{\Delta t_k^2}{2} \tilde{q}_y & 0 & \Delta t_k \tilde{q}_y \end{pmatrix}$$

with $\Delta t_k = t_{k+1} - t_k$.

The measurement model is

$$z(t_k) = h(\xi^-(t_k)) + r(t_k) \quad (32)$$

where $z(t_k)$ is the measurement and the measurement noise $r(t_k)$ is modeled by a white, mean-free Gaussian process with covariance matrix $R(t_k)$. The example measurement function h is given by typical radar measurements (r, ϕ, \dot{r}) , i. e.

$$h(\xi) = \begin{pmatrix} \sqrt{x^2 + y^2} \\ \arctan\left(\frac{y}{x}\right) \\ \frac{x\dot{x} + y\dot{y}}{\sqrt{x^2 + y^2}} \end{pmatrix} \quad (33)$$

and $H = \frac{\partial h}{\partial \xi}$ is its linearization.

For the illustration of our main results in the numerical study we have chosen a linear dynamical model with a time-dependent control input that can be solved in closed form for both the prediction of the mean and the covariance matrix. However, this dynamical system above is just an example to illustrate the application of the results in sec. V-A to a concrete setup; other in general non-linear dynamical systems and state vectors can be used as long as they contain relative position and its first derivative.

C. Evaluation of the 2D integral for the entry intensity

The integral

$$\int_{\dot{x} \leq 0} \int_{y \in I_y} \dot{x} p_t(y, \dot{x}|x_0) dy d\dot{x} \quad (34)$$

in eq. (21) for the entry intensity cannot be computed in closed form if the covariance matrix of $p_t(y, \dot{x}|x_0)$ is not diagonal. Instead of a full numerical 2D integration scheme we Taylor-expand the 2D pdf with respect to the off-diagonal element of the *inverse* covariance matrix around 0 to a certain order and then integrate. For a general 2D Gaussian pdf $p(x_1, x_2) = \mathcal{N}(\xi; \mu, \Sigma)$ with $\xi = (x_1, x_2)^\top$ and mean μ and covariance matrix Σ the Taylor-expansion to linear order with respect to Σ_{12}^{-1} reads

$$\begin{aligned} \mathcal{N}(\xi; \mu, \Sigma) &= \mathcal{N}\left(x_1; \mu_1, \sqrt{\tilde{\Sigma}_{11}}\right) \mathcal{N}\left(x_2; \mu_2, \sqrt{\tilde{\Sigma}_{22}}\right) \\ &\quad - \Sigma_{12}^{-1} \left((x_1 - \mu_1) \mathcal{N}\left(x_1; \mu_1, \sqrt{\tilde{\Sigma}_{11}}\right) \right. \\ &\quad \cdot \left. \left((x_2 - \mu_2) \mathcal{N}\left(x_2; \mu_2, \sqrt{\tilde{\Sigma}_{22}}\right) \right) \right) \\ &\quad + \mathcal{O}\left((\Sigma_{12}^{-1})^2\right) \end{aligned}$$

with $\Sigma_{12}^{-1} = -\frac{\Sigma_{12}}{|\Sigma|}$ and $\tilde{\Sigma}_{11} = \frac{|\Sigma|}{\Sigma_{22}}$, $\tilde{\Sigma}_{22} = \frac{|\Sigma|}{\Sigma_{11}}$. This leads to the following integral

$$\begin{aligned} & \int_{x_{1l}}^{x_{1u}} \int_{x_{2l}}^{x_{2u}} x_1 p(x_1, x_2) dx_1 dx_2 = \\ & \left[\frac{\mu_1}{2} \operatorname{erf} \left(\frac{x_1 - \mu_1}{\sqrt{2\tilde{\Sigma}_{11}}} \right) - \tilde{\Sigma}_{11} \mathcal{N} \left(x_1; \mu_1, \sqrt{\tilde{\Sigma}_{11}} \right) \right]_{x_{1l}}^{x_{1u}} \cdot \\ & \quad \cdot \left[\frac{1}{2} \operatorname{erf} \left(\frac{x_2 - \mu_2}{\sqrt{2\tilde{\Sigma}_{22}}} \right) \right]_{x_{2l}}^{x_{2u}} \\ & - \Sigma_{12}^{-1} \left[x_1 \tilde{\Sigma}_{11} \mathcal{N} \left(x_1; \mu_1, \sqrt{\tilde{\Sigma}_{11}} \right) - \frac{\tilde{\Sigma}_{11}}{2} \operatorname{erf} \left(\frac{x_1 - \mu_1}{\sqrt{2\tilde{\Sigma}_{11}}} \right) \right]_{x_{1l}}^{x_{1u}} \cdot \\ & \quad \cdot \left[\tilde{\Sigma}_{22} \mathcal{N} \left(x_2; \mu_2, \sqrt{\tilde{\Sigma}_{22}} \right) \right]_{x_{2l}}^{x_{2u}} + \mathcal{O}((\Sigma_{12}^{-1})^2) \end{aligned}$$

We expand with respect to the off-diagonal entry of the inverse covariance since this is the element that prevents factorization into one-dimensional Gaussians. We have checked that Taylor-expansion with respect to the off-diagonal entry of the covariance matrix leads to less accurate results to first order.

D. Entry intensity for circular boundary

For a circular boundaries it is advantageous to work with a pdf in polar coordinates $\tilde{p}_t(r, \phi, \dot{r}, \dot{\phi})$. Then application of eq. (14) to an entry boundary crossing of a circle with radius r_0 yields the following entry intensity:

$$\mu^+ (\Gamma_{circ}, t) = - \int_{\phi=0}^{2\pi} \int_{\dot{r} \leq 0} \int_{\dot{\phi} \in \mathbb{R}} \dot{r} \tilde{p}_t(r_0, \phi, \dot{r}, \dot{\phi}) d\phi d\dot{r} d\dot{\phi} \quad (35)$$

If the distribution is initially formulated in Cartesian coordinates, i. e. $p_t(x, y, \dot{x}, \dot{y})$, a coordinate transformation must be applied:

$$\begin{aligned} & \tilde{p}_t(r, \phi, \dot{r}, \dot{\phi}) = \\ & r^2 p_t \left(r \cos \phi, r \sin \phi, \dot{r} \cos \phi - r \dot{\phi} \sin \phi, \dot{r} \sin \phi + r \dot{\phi} \cos \phi \right) \end{aligned}$$

REFERENCES

- [1] J. Jansson and F. Gustafsson, "A framework and automotive application of collision avoidance decision making," *Automatica*, vol. 44, no. 9, pp. 2347–2351, 2008.
- [2] M. M. Muntzinger, S. Zuther, and K. Dietmayer, "Probability estimation for an automotive pre-crash application with short filter settling times," in *Proceedings of IEEE Intelligent Vehicles Symposium*, 2009, pp. 411–416.
- [3] J. E. Stellet, J. Schumacher, W. Branz, and J. M. Zöllner, "Uncertainty propagation in criticality measures for driver assistance," in *Intelligent Vehicles Symposium (IV), 2015 IEEE*. IEEE, 2015, pp. 1187–1194.
- [4] J. Jansson, "Collision avoidance theory: With application to automotive collision mitigation," Ph.D. dissertation, Linköping University Electronic Press, 2005.
- [5] A. Lambert, D. Gruyer, and G. Saint Pierre, "A fast monte carlo algorithm for collision probability estimation," in *Control, Automation, Robotics and Vision, 2008. ICARCV 2008. 10th International Conference on*. IEEE, 2008, pp. 406–411.
- [6] M. Prandini, J. Hu, J. Lygeros, and S. Sastry, "A probabilistic approach to aircraft conflict detection," *IEEE Transactions on intelligent transportation systems*, vol. 1, no. 4, pp. 199–220, 2000.

- [7] P.-J. Nordlund and F. Gustafsson, *Probabilistic conflict detection for piecewise straight paths*. Linköping University Electronic Press, 2008.
- [8] A. Genz, "Numerical computation of rectangular bivariate and trivariate normal and t probabilities," *Statistics and Computing*, vol. 14, no. 3, pp. 251–260, 2004.
- [9] G. Lindgren, *Stationary stochastic processes: theory and applications*. CRC Press, 2012.
- [10] H. R. Lerche, *Boundary crossing of Brownian motion: Its relation to the law of the iterated logarithm and to sequential analysis*. Springer Science & Business Media, 2013, vol. 40.
- [11] Y. K. Belyaev, "On the number of exits across the boundary of a region by a vector stochastic process," *Theory of Probability & Its Applications*, vol. 13, no. 2, pp. 320–324, 1968.
- [12] R. Altendorfer, "Observable dynamics and coordinate systems for automotive target tracking," in *Proceedings of IEEE Intelligent Vehicles Symposium*, 2009, pp. 741–746.
- [13] Y. Bar-Shalom, X. R. Li, and T. Kirubarajan, *Estimation with Applications to Tracking and Navigation*. Wiley, 2001.